Excess pCO2 in Surface Seawater of the Arabian Gulf

James W. Murray[1], Jassem Al-Thani[2], Oguz Yigiterhan[2], Ebrahim Mohd Al-Ansari[2],
Vethamony Ponnumony[2], Caesar Flonasca Sorino[2], and Daniel B Anderson[1]

[1]University of Washington
[2]Qatar University

November 23, 2022

Abstract

Dissolved inorganic carbon (DIC) and total alkalinity (TA) were sampled in December, 2018 and May, 2019 in the Exclusive Economic Zone (EEZ) of Qatar in the Arabian Gulf. pCO_2 calculated in surface seawater averaged 459 ± 61 matm and was supersaturated with respect to the atmosphere. The region was degassing CO_2 to the atmosphere and the flux was about 1.25 mmol C m^{-2} d^{-1}. The origin of this excess CO_2 must be due to $CaCO_3$ precipitation. The horizontal relationship between salinity-normalized total alkalinity (NTA) and dissolved inorganic carbon (NDIC) showed that $CaCO_3$ formation was more important, relative to net biological productivity, than in the open ocean. The tracer Alk* has values primarily determined by $CaCO_3$ formation and values of Alk* ranged from -50 to -310 mmol kg^{-1}, which is consistent with substantial $CaCO_3$ formation. DAlk* increased with increasing distance northward from Hormuz. The rate of calcification calculated from the air-sea flux of CO_2 (5.6 mmol C kg^{-1} y^{-1}) and from DAlk* (5.9 mmol C kg^{-1} y^{-1}) agreed well. However, $CaCO_3$ formation by net calcification in coral reefs is unlikely as they have limited distribution and have been severely damaged by past coral bleaching. There are high concentrations of excess particulate Ca in the water column that cannot be accounted for by input of $CaCO_3$-rich Qatari dust. Carbonate forming plankton are absent in the water column. We propose that abiological, heterogeneous calcite precipitation (HCP) may be occurring. The mechanism is unknown but nucleation by $CaCO_3$-rich Qatari dust may assist this process.

Excess pCO_2 in Surface Seawater of the Arabian Gulf

Izumi, Connor[1];
Al-Thani, Jassem[2];
Yigiterhan, Oguz[2];
Al-Ansari, Ebrahim Mohd A S [2];
Vethamony, Ponnumony [2];
Sorino, Caesar Flonasca [2];
Anderson, Daniel B. [1];
Murray, James W. [1]*

1. School of Oceanography, University of Washington,
   Box 355351, Seattle WA 98195, USA

2. Environmental Science Center, Qatar University,
   P.O. Box: 2713, Al-Tarfa, Doha, Qatar

*Corresponding Author
James W. Murray
School of Oceanography,
University of Washington,
Box 355351,
Seattle WA 98195
jmurray@uw.edu

Running head: Excess pCO_2

Key Points

1. pCO_2 in surface seawater in the Arabian Gulf averages about 460 µatm and is supersaturated with respect to the atmosphere

2. Salinity normalized total alkalinity (NTA) and dissolved inorganic carbon (NDIC), and the tracer ΔAlk*, suggest that $CaCO_3$ formation is the origin of this excess CO_2.

3. $CaCO_3$ formation in coral reefs is unlikely due to bleaching events and abiological heterogeneous calcite precipitation in the water column may be occurring.

ABSTRACT:

Dissolved inorganic carbon (DIC) and total alkalinity (TA) were sampled in December, 2018 and May, 2019 in the Exclusive Economic Zone (EEZ) of Qatar in the Arabian Gulf. pCO_2 calculated in surface seawater averaged 459 ± 61 μatm and was supersaturated with respect to the atmosphere. The region was degassing CO_2 to the atmosphere and the flux was about 1.25 mmol C m^{-2} d^{-1}. The origin of this excess CO_2 must be due to $CaCO_3$ precipitation. The horizontal relationship between salinity-normalized total alkalinity (NTA) and dissolved inorganic carbon (NDIC) showed that $CaCO_3$ formation was more important, relative to net biological productivity, than in the open ocean. The tracer Alk* has values primarily determined by $CaCO_3$ formation and values of Alk* ranged from -50 to -310 μmol kg^{-1}, which is consistent with substantial $CaCO_3$ formation. ΔAlk* increased with increasing distance northward from Hormuz. The rate of calcification calculated from the air-sea flux of CO_2 (5.6 mmol C kg^{-1} y^{-1}) and from ΔAlk* (5.9 mmol C kg^{-1} y^{-1}) agreed well. However, $CaCO_3$ formation by net calcification in coral reefs is unlikely as they have limited distribution and have been severely damaged by past coral bleaching. There are high concentrations of excess particulate Ca in the water column that cannot be accounted for by input of $CaCO_3$-rich Qatari dust. Carbonate forming plankton are absent in the water column. We propose that abiological, heterogeneous calcite precipitation (HCP) may be occurring. The mechanism is unknown but nucleation by $CaCO_3$-rich Qatari dust may assist this process.

250 / 250 words

Data Availability

The data used for preparing this study has been submitted to BCO-DMO and is being processed,

71

72 **Plain Language Summary (<200 words)**

73

74 Ocean acidification is a consequence of increased emissions of CO_2 to the atmosphere and is a

75 major threat to marine ecosystems. Coral reefs in the Arabian Gulf have historically been a

76 significant component of this warm and salty region's marine biological storehouse. Though

77 ocean acidification is a concern, little is known about the carbonate system chemistry in these

78 waters. The most recent previous data was from 1977 and techniques have improved since that

79 time. An international collaboration between Qatar University and the University of Washington

80 provided an opportunity to correct this deficiency. Samples for dissolved inorganic carbon and

81 total alkalinity were collected in December, 2018 and May 2019. Values of pCO_2 in surface

82 seawater were greater than atmospheric values indicating that the Gulf was not taking up

83 atmospheric CO_2. Horizontal changes in DIC and TA indicate that $CaCO_3$ formation is

84 occurring. The origin of the elevated pCO_2 must be due to $CaCO_3$ formation. However, carbonate

85 forming plankton are not present and coral reefs, though abundant in the past, have been severely

86 damaged by several bleaching events. One possible explanation is that abiological $CaCO_3$

87 formation is occurring in the water column, perhaps assisted by nucleation on $CaCO_3$-rich dust

88 of land-based origin.

89
90 200/200 words
91
92
93

111   **1. Introduction**

112   There is concern that coral reefs in the Arabian (Persian) Gulf (hereafter referred to as

113   'Gulf') are being severely impacted by ocean acidification (Orr et al., 2005; Doney et al., 2009)

114   yet little is known about the carbonate system geochemistry in this region. Reefs cover a

115   relatively small area but they represent the region's biological storehouse. Many of the Gulf's

116   fisheries depend on these habitats. It comes as a surprise to many that the Gulf is a repository of

117   significant biodiversity. Historically, the countries bordering the Gulf exploited pearl oyster beds

118   and coral reefs as a large part of their economy and cultural heritage. The World-Wide Fund for

119   Nature (WWF) has identified the Gulf as part of a Global 200 Ecoregion - one of 43 priority

120   marine ecosystems worldwide. Unfortunately, the coral reefs in this region have been severely

121   impacted by degradation due to climate change and anthropogenic modifications.

122   The Gulf is a semi-enclosed marginal sea with an area of 240,000 km^2 and mean depth of

123   35m (Kampf and Sadrinasab, 2006; Vaughan et al., 2019). Most deeper areas of the Gulf are

124   located along the Iranian coast whereas broad, shallow regions with depths less than 35 m are

125   found along the coast of Arabian Peninsula. It has free exchange with the Gulf of Oman in the

126   Arabian Sea through the Strait of Hormuz, which is 56 km wide and has a maximum depth of

127   100m (Al Ansari et al., 2015). The circulation in the Gulf is characterized as reverse estuarine.

128   Lower salinity (S = 36.5) seawater enters at the surface through the Strait of Hormuz. The

129   climate of this regions is very hot and dry and evaporation is estimated to be ~200 cm yr^{-1} for the

130   central region of the Gulf (Al Ansari et al., 2015). Hence, the salinity and density increase due to

131   evaporation as seawater flows to the north from the Strait. Higher salinity seawater (S $\geq$ 40) exits

132   at depth through the Strait. Due to geostrophy, the inflow of Indian Ocean Surface Water

133   (IOSW) follows the Iranian coastline, whereas the denser bottom outflow follows the coastline of

5

134   the United Arab Emirates. The total volume of the Gulf is ~8,600 km^3 and the volume of the

135   deep outflow through Hormuz is about 6,620 km^3 y^{-1}. Therefore, the total residence time of the

136   Gulf's seawater is about 1.3 years (Sheppard et al., 2010). Residence time is a crucial factor

137   when considering the status of ocean acidification. Concentrations of carbonate system species in

138   the surface waters reflect a balance between the inputs through the Straits, enrichment due to

139   evaporation and the sources and sinks due to air-sea exchange and biological processes.

140   The carbonate system chemistry in the Gulf was first sampled in 1977 (Brewer and

141   Dyrssen, 1985) but has not been studied since. Surface water enters the Gulf with relatively high

142   concentrations of dissolved inorganic carbon (DIC) and total alkalinity (TA) from the Arabian

143   Sea. As the water flows northward, DIC and TA increase but salinity normalized DIC (NDIC)

144   and alkalinity (NTA) decrease. The decrease in concentrations of NDIC and NTA can be used to

145   determine the relative importance of CO_2 removal by $CaCO_3$ formation versus primary

146   production. Another factor to consider is that, as the water flows northward, some CO_2 is lost to

147   the atmosphere due to gas exchange. At the time of the Brewer and Dyrssen study in 1977, the

148   Arabian Gulf was degassing CO_2 to the atmosphere. Now, 40 years have passed and the

149   gradients and fluxes may have changed. Because data regarding the progress of ocean

150   acidification in the Arabian Gulf are sparse, an international collaboration between Qatar

151   University (QU) and the University of Washington (UW) provided an opportunity to alleviate

152   this deficiency.

153   The goal of this study was to assess the status of the ocean carbonate system in the

154   Exclusive Economic Zone of Qatar in the Arabian Gulf with respect to present and future

155   impacts by ocean acidification and use the horizontal distributions of DIC and TA to determine

156 the relative importance of organic matter production and $CaCO_3$ formation as sinks and sources

157 of CO_2.

158 **2. Methods**

159 **2.1 Samples**

160 Water column sampling was conducted, using 12, rosette mounted, 10-L PVC Niskin

161 bottles, on December 5, 2018 and May 18, 2019 in the Arabian Gulf on the RV Janan (Figure 1).

162 Surface seawater samples and hydrographic data were collected at seven stations (stations 1C,

163 2C, 3C, 4C, 5C, 6B, 6C) along a transect from the central east coast of Qatar across the Qatari

164 Exclusive Economic Zone (EEZ). Stations were chosen to be nearly perpendicular to the major

165 axis of the Gulf to capture main regional hydrographic features across the EEZ. The transect

166 provides a reasonable representation of hydrographic distributions across the wider part of the

167 Gulf. Samples were collected in triplicate at each station. Vertical profiles with one surface

168 sample, one bottom sample, and 1 to 3 mid-depth samples were collected at stations 2C, 4C, 6B,

169 and 6C.

170 Samples for DIC and TA were collected in 300 mL Wheaton BOD glass bottles with

171 ground glass stoppers. Samples were sealed immediately after collection to prevent loss of CO_2.

172 Samples were poisoned with 150 µL $HgCl_2$ (0.05% by volume) to prevent biological activity,

173 then covered with aluminum foil.

174

175

176 **2.2 Analyses**

177 The best approach for understanding ocean acidification is to measure the primary

178 capacity factors of the carbonate system chemistry which are dissolved inorganic carbon (DIC)

179 and total alkalinity (TA) (Stumm and Morgan, 1995). Being capacity factors means that they

180 behave conservatively during mixing, in the absence of gas exchange and biological processes.

181 DIC and TA may not be the most precise pair of variables for calculating pH, pCO_2 and

182 carbonate ion (Orr et al, 2018) but they were the most convenient parameters for us to measure

183 on samples collected in the Arabian Gulf and shipped to Seattle for analyses.

184   After collection, samples were shipped to the University of Washington for DIC and TA

185 analyses in Dr. Alex Gagnon's laboratory. Carbonate system measurements followed the

186 methods of Dickson et al. (2007). Briefly, TA (μmol kg^{-1}) was determined through open-cell

187 automated titration (876 Dosimat plus, Metrohm AG) with a 0.1M hydrochloric acid

188 (HCl)+0.6M sodium chloride (NaCl) solution. Total DIC (μmol kg^{-1}) was obtained through

189 coulometric determination (VINDTA 3D, Marianda with UIC coulometer). Certified reference

190 materials for TA and DIC obtained from Andrew Dickson (Scripps Institution of Oceanography)

191 were run in conjunction with seawater samples as a calibration standard and to monitor

192 precision. Long-term precision for DIC and TA in this lab, based on repeated measurements of

193 CRM materials, was $\pm$ 3.7 μmol kg^{-1} (2σ std. dev.) and $\pm$ 4.3 μmol kg^{-1} (2σ std. dev.),

194 respectively (Bolden et al., 2019).

195   pCO_2, pH and CO_3^{2-} were calculated from DIC and TA using CO2Calc on the total pH

196 scale with carbonate equilibrium constants refit from Mehrbach et al. (1973) by Dickson and

197 Millero (1987); borate alkalinity was calculated using the boron / chlorinity (salinity)

198 relationship provided by Lee et al. (2010) and equilibrium constants from Dickson (1990).

199 Where necessary, TA, and DIC values used in subsequent calculations were salinity-normalized

200 (NTA, NDIC) to a mean salinity value of 40.0. As there are no significant freshwater

201 contributions from rivers or groundwater in this region, the normalization relationship of Friis et

202   al (2003) was not necessary. During both cruises, hydrographic properties (temperature,

203   practical salinity (S_p), O_2, pH, % transmission and fluorescence) were measured using a SeaBird

204   Electronics, SBE 911 mounted on a SeaBird rosette. The pH sensor used in our project was a

205   SBE 27 pH / O.R.P (Redox) Sensor. Dissolved oxygen was measured using the SBE 43

206   Dissolved Oxygen sensor. Discrete water samples were taken directly from the Niskin bottles

207   and analyzed for dissolved oxygen within a few hours of collection using the Winkler titrimetric

208   method (Carpenter, 1965). Nutrients (NO_3, NO_2, NH_4, soluble reactive phosphate (SRP) and Si)

209   and chlorophyll were analyzed on filtered samples using classical techniques (Parsons et al.,

210   1984).

211   Suspended particulate matter for particulate Ca analyses was sampled in 2012, at the

212   same stations, on a previous cruise. Seawater was filtered directly from Niskin bottles through 47

213   mm filter holders and 0.45 µM mesh size Nuclepore filters (Yigiterhan et al., 2020). Filtration

214   volumes of 2 L, provided sufficient samples for analyses. Particulate samples were acid digested

215   in a clean lab on hot plates using trace metal grade concentrated HF (16.5M), HCl (6M) and,

216   HNO_3 (16M) acids (Yigiterhan and Murray, 2008; Yigiterhan et al., 2011). H_2O_2 was added for

217   complete removal of the organic material. Calcium analyses were done using ICP-OES with

218   precision and accuracies of about 5%. Excess Ca concentrations (non-lithogenic) were

219   calculated, as in Yigiterhan et al. (2020), by subtracting the lithogenic fraction using aluminum

220   as a tracer and assuming that the composition of the lithogenic fraction can be represented by

221   composition of average dust from Qatar (Yigiterhan et al., 2018).

222        $$Ca_{excess} = Ca_{total} - Al_{total} \ x \ Ca/Al_{dust} \qquad (1)$$

223

224

225   3. Results

226   The hydrographic (Station, Depth, T, S_p, O_2), nutrient (NO_3, SRP, H_4SiO_4) and carbonate

227   system (DIC, TA) data are given in Table 1. Calculated pCO_{2calc} and pH_{calc} are also given in

228   Table 1. The means and standard deviations are given for each cruise. As there was no statistical

229   difference between the data from the two cruises, the data sets were combined for the

230   interpretations.

231   Temperature ranged from 24.458° to 26.845°C and salinity (S_p) ranged from 40.290 to

232   40.994. DIC content ranged from 2065 to 2235 μmol kg^{-1}, and TA levels ranged from 2415 to

233   2601 μmol kg^{-1}. There was no systematic variation observed with depth. The nutrient

234   concentrations were very low reflecting the oligotrophic nature of this water column. The

235   regression of NO_3 versus SRP is not significant with $R^2 = 24\%$ (not shown). But, comparison of

236   the measured data with the Redfield relationship (NO_3/SRP = 15) showed that the water column

237   was nitrate deficient. This condition often favors nitrogen fixation (e.g., Deutsch et al., 2007),

238   which has not been previously studied in the Gulf. Oxygen concentrations ranged from 176 to

239   202 μmol kg^{-1}, NO_3^- varied from 0.57 to 2.40 μmol kg^{-1}, NO_2^- from 0.09 to 1.44 μmol kg^{-1}, SRP

240   from 0.06 to 0.93 μmol kg^{-1}, and dissolved silicate from 0.40 to 3.65 μmol kg^{-1}. % transmission

241   ranged from 70.621% to 95.530%. Fluorescence ranged from 0.209 to 1.423, and chlorophyll

242   levels ranged from 0.81 to 2.07 μgm kg^{-1}.

243   pCO_2, pH and CO_3^{2-} were calculated from DIC and TA. The pH measured by the SeaBird

244   pH sensor (NBS scale) varied, from 8.13 to 8.22, but the pH_{calc} calculated from DIC and TA

245   (total H scale) ranged between 7.93 and 8.12. Though accessible, pH sensors (SeaFET) can be

246   inaccurate if sensor handling and calibration is not done with care (Miller et al., 2018). Because

247   of these uncertainties, we used the values of pH_{calc} in this study. Calculated pCO_2 ranged from

248   390 to 582 μatm. The water column was supersaturated with respect to calcite ($\Omega_{calcite}$ = 4.97 to

249   6.95) and aragonite ($\Omega_{aragonite}$ = 3.32 to 4.62).

250   **4. Discussion**

251   **4.1 pCO$_2$ in Surface Seawater**

252   The partial pressures of carbon dioxide (pCO$_2$) in surface water of the Qatari EEZ in the

253   central Arabian Gulf were higher than atmospheric pCO$_2$ during these study periods. The average

254   surface concentrations were 478±80 μatm in November 2018 and 442±30 μatm in May 2019.

255   Hence, the Gulf is a source of CO$_2$ to the atmosphere. Ocean acidification by local oceanic

256   uptake of atmospheric CO$_2$ is not presently occurring. If atmospheric CO$_2$ continues to increase

257   at its present rate the air-sea gradient will reverse and oceanic uptake of CO$_2$ will occur in

258   approximately 2042. The question is "why are these surface waters supersaturated with CO$_2$?"
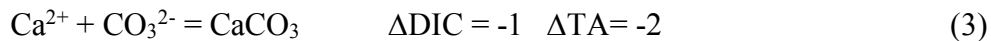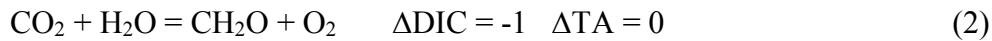
259   It is possible that the surface seawater entering through the Strait of Hormuz from the

260   Gulf of Oman has been impacted by ocean acidification, resulting in higher DIC than pre-

261   acidification. Thus, we can't absolutely rule out any impact from ocean acidification.

262   Unfortunately, the source seawaters vary seasonally and their T, S and carbonate system

263   compositions, appropriate for our study, are not available.

264   **4.2 Alkalinity and DIC**

265   The concentration of pCO$_2$ in seawater is controlled by the relative concentrations of

266   carbonate Alk versus DIC. The relationship between TA and DIC in the Qatari EEZ is shown in

267   Figure 2. There is essentially no statistical difference between the average values of TA and DIC

268   for the two different sampling periods but we identify them separately in the figure. They were

269   combined for the data analysis. Also shown are concentrations in the inflowing surface water at

270   the Strait of Hormuz, which we assumed were the same as in Brewer and Dyrssen (1985). Both

271   TA and DIC increase after entering the Arabian Gulf, due to the increase in salinity due to

272   evaporation.

273   To interpret the geochemistry of the carbonate system we normalizing individual

274   concentrations to a constant salinity (S = 40). The resulting normalized values of NTA and NDIC

275   are plotted in Figure 3. We also show the surface water concentrations from the Strait of Hormuz

276   and the surface data, from 1977, in the Gulf from Brewer and Dyrssen (1985). The

277   concentrations of NTA and NDIC decrease as surface seawater flows to the north after entering

278   through Hormuz from the Arabian Sea. The combined data sets decrease with a slope of

279    $\Delta NTA/\Delta NDIC = -0.65$. If we assume simple model reactions for formation of organic matter

280   (CH_2O) and $CaCO_3$, the change in $CaCO_3$ formation and organic matter production can be

281   predicted.

282

283            $CO_2 + H_2O = CH_2O + O_2$ $\Delta DIC = -1$ $\Delta TA = 0$ (2)

284             $Ca^{2+} + CO_3^{2-} = CaCO_3$ $\Delta DIC = -1$ $\Delta TA = -2$ (3)

285

286   The observed changes in NTA and NDIC, as surface seawater moves from the Strait of Hormuz

287   to the Qatari EEZ, are consistent with a ratio of carbon uptake by $CaCO_3$ formation to carbon

288   uptake by net photosynthesis ($\Delta CaCO_3 / \Delta OrgC$) of slightly greater than 0.6 (a ratio of about

289   1:2). For comparison, the average ratio for open ocean surface seawater, using this same

290   approach, is about 1:18 (Emerson and Hedges, 2012). Therefore, carbon removal by $CaCO_3$

291   formation, relative to net photosynthesis, in the Gulf is about 12 times larger than in the open

292   ocean.

293   This estimate neglects loss of CO_2 to the atmosphere by gas exchange and uptake by net

294   biological production. The characteristic residence time for gas exchange of CO_2 is slow, on the

295   time scale of one year. The residence time for the whole Arabian Gulf is about 1.3 years. Thus,

296   while we assume that loss of CO_2 is minor, some of the decrease in $\Delta NDIC$ may be due to gas

297   exchange and our estimates of the $\Delta CaCO_3$ / $\Delta OrgC$ should be considered an upper limit.

298   pCO_2 also becomes elevated in hypersaline reverse estuaries (e.g., Yao et al., 2020), but

299   as pCO_2 is controlled by the ratio of DIC / TA, it reflects DIC and TA consumption processes,

300   not the increase in S alone. Though S increases from S = 36.5 in the Gulf of Oman to S = 40.5 in

301   the Qatari EEZ this would not be considered a hypersaline environment.

302   The data from 1977 and 2018/2019 agree well. There has been no systematic change in

303   most of the NTA or NDIC data. The exception is that NTA in the 1977 data were lower for

304   NDIC concentrations less than ~2140 $\mu mol\ kg^{-1}$. These data are from the shallower region in the

305   Arabian Gulf to the NW of Qatar which may be anomalous because of freshwater input from

306   rivers in Kuwait. The ratio of $\Delta CaCO_3$ to $\Delta OrgC$ in 1977 of 2.5 was larger than for our combined

307   data sets in 2020, suggesting greater $CaCO_3$ removal in 1977 (Brewer and Dyrssen, 1985). That

308   may be because the Brewer and Dyrssen (1985) data included samples from the northwestern

309   part of the Arabian Gulf or it may suggest that $CaCO_3$ removal has decreased over the past

310   43years.

311   The slope of ΔNTA / ΔDIC (-0.65), and the corresponding $\Delta CaCO_3$ / $\Delta OrgC$ removal

312   ratios (1:2), can also be compared to those measured in healthy coral reef systems, elsewhere. In

313   the eastern central Red Sea, at Al-Fahal reef, the regression between NTA and NDIC was -0.42

314   (Saderne et al., 2019). This slope closely corresponds to the mean of the global coral reefs of

315   -0.41± 0.18 (Cyronak et al., 2018). A slope of 0.4 corresponds to $\Delta CaCO_3$ / $\Delta OrgC$ = 0.25. In

316   other words, one CaCO₃ removed per four organic carbon. At other locations, not strictly

317   comparable with the Arabian Gulf, a removal ratio of 2 was observed in the pristine Tetiaroa

318   Coral Atoll (Bolden et al., 2019) and a ratio of 2.3 was calculated for the coral reef system in

319   Kaneohe Bay, Hawaii (Fagan and Mackenzie., 2007). Though important, removal of C as CaCO₃

320   plays less of a role in the Gulf, than in healthy reef locations.

321   **4.3 Alk***

322   The tracer Alk* has values primarily determined by $CaCO_3$ precipitation and dissolution

323   (Carter et al., 2014). To define Alk**,** potential alkalinity (A_P) is calculated first to remove the

324   influence of nitrification (Brewer et al., 1975). Carter et al (2014) used an empirical relationship

325   that includes the combined effect of nitrate, sulfate and SRP (Kanamori and Ikegami, 1982).

326   Though derived for the North Pacific, this coefficient appears to be globally applicable (Wolf-

327   Gladrow et al., 2007). Potential alkalinity (A_P) is defined as:

328

329                    $$A_P = TA + 1.26\ [NO_3] \tag{4}$$

330

331   where TA is total alkalinity and $[NO_3]$ is the concentration of nitrate ($\mu mol\ kg^{-1}$). To remove the

332   dependence on salinity, a background concentration, conservative potential alkalinity (A_P^C), is

333   calculated as:

334                    $$A_P^C = S\ \frac{A'_P}{S'} = S \times 66.40\ \mu mol\ kg^{-1} \tag{5}$$

335

336   where A'_P and S' are mean values for the whole surface ocean. Though our data is from a coastal

337   region, we assume this equation can be utilized as fresh water input is negligible. Carter et al

338   (2014) defined Alk* as the deviation of potential alkalinity from A_P^C.

339

$$\text{Alk*} = A_P - A_P^C \tag{6}$$

341

$$= A_P - S \times 66.40 \ \mu\text{mol kg}^{-1} \tag{7}$$

343

Regions with large net carbonate precipitation result in negative Alk*. All values of Alk*

calculated for our data set were negative and ranged from -50 to -310 $\mu\text{mol kg}^{-1}$. This is

consistent with substantial $CaCO_3$ formation in the Gulf. The Alk* values calculated using the

same equations, by Carter et al. (2014) for the Red Sea and the Trucial Coast region (the Pirate

Coast) of Oman in the Arabian Gulf were -247 $\mu\text{mol kg}^{-1}$ and -240 $\mu\text{mol kg}^{-1}$, respectively.

In order to examine the spatial variability of how much $CaCO_3$ was precipitating in the

Arabian Gulf itself, we calculated ΔAlk*, the difference between the specific locations in the

Qatari EEZ and the surface water entering through the Strait of Hormuz. ΔAlk* increased with

increasing distance northward from Hormuz to values as large as -310 $\mu\text{mol kg}^{-1}$ (Figure 4). The

average decrease of Alk* was -130 $\mu\text{mol kg}^{-1}$, which corresponds to a calcification of -65 μmol

kg^{-1}.

The slope of ΔNTA versus ΔNDIC (corresponding to $\Delta CaCO_3/\Delta OrgC = 1:2$) and the

negative values of Alk* suggest that large amounts of $CaCO_3$ are precipitating. This reaction,

forming one mol of $CaCO_3$ produces one mole of CO_2 (equation 8), can explain why the

concentrations of pCO_2 in the surface water are supersaturated.

359

$$2\ HCO_3^- + Ca^{2+} = CaCO_3 \downarrow + CO_2 \uparrow + H_2O \tag{8}$$

361

362   The precipitation of $CaCO_3$ is promoted by the elevated of the waters with respect to calcite

363   ($\Omega_{calcite}$ = 4.97 to 6.95) and aragonite ($\Omega_{aragonite}$ = 3.32 to 4.62).

364

365   **4.4 Air-Sea Flux of CO_2**

366   We calculated the flux of CO_2 across the air - sea interface as an estimate of the rate of

367   calcification. The flux was calculated using the stagnant boundary layer model for gas exchange

368   (e.g., Liss and Slater, 1974).

369

370                    $$Flux_{CO2} = k \, K_H \, (pCO_{2sw} - pCO_{2atm}) = K \, \Delta pCO_2 \qquad (9)$$

371

372   where k is the piston velocity (a function of wind speed), K_H is the solubility of CO_2 in seawater

373   (a function of T and S_p) and ΔpCO_2 is the gradient of CO_2 across the air-sea interface. We

374   assumed the annual average wind speed at Doha, Qatar of 8 knots (~4 m s^{-1}) (from Qatar Civil

375   Aviation Authority, https://qweather.gov.qa/ClimateInfo.aspx) which corresponds to a piston

376   velocity of k = 5 cm h^{-1} or 1.25 m d^{-1} (Wanninkhof, 1992). The solubility (K_H) of CO_2 for T =

377   25°C and S_p = 40 is about 20 x 10^{-3} mol kg^{-1} atm^{-1}. We assumed the average pCO_2 in surface

378   seawater was 450 µatm and atmospheric pCO_2 was 400 µatm and therefore, ΔpCO_2 = 50 µatm.

379   The resulting flux of CO_2 was -1.25 mmol C m^{-2} d^{-1} or -0.46 mol C m^{-2} y^{-1}. This is an

380   approximate calculation because it assumes representative concentrations and an average wind

381   speed. However, wind speed is variable and the relationship between k and windspeed is not

382   linear. It is also only an approximation as we only have two time points in the annual cycle.

383   During calcification, seawater becomes more acid due to the removal of bicarbonate and

384   carbonate ions, and this change in pH increases the abundance of dissolved CO_2 (Stumm and

16

385 Morgan 1995). The partial pressure of CO_2 increases and, in an open system, the CO_2 produced

386 is either taken up by biological production or escapes to the atmosphere. This simplistic

387 representation of the calcification process suggests that for each mole of $CaCO_3$ deposited, a

388 mole of CO_2 is liberated (Eqn. 8). The relationship is about 1:1 in freshwater but is reduced in

389 buffered seawater where only approximately 0.62 moles of CO_2 are liberated per mole of $CaCO_3$

390 deposited (Ware et al., 1991). Calculations show that the amount of CO_2 that must be released to

391 equilibrate seawater increases with increasing partial pressure of CO_2 in seawater (pCO_2)

392 (Frankignoulle et al., 1994). The calculation of the rate of calcification given here could be a

393 lower limit because we neglect CO_2 uptake by net biological production or could be an upper

394 limit as we neglect respiration of dissolved and particulate organic carbon.

395   If this calcification occurred in the water column with an average depth of 50m, the

396 volume rate would be 0.015 μmol kg^{-1} d^{-1} or 5.6 μmol C kg^{-1} y^{-1}. We can compare this with the

397 average decrease in Alk* of ΔAlk* = 130 μmol kg^{-1} (Section 4.3) which corresponds to a $CaCO_3$

398 formation rate of 65 μmol kg^{-1}. If we assume the seawater has a residence time of 1.3 years

399 (Sheppard et al., 2010), the $CaCO_3$ formation rate would be 5.0 μmol C kg^{-1} y^{-1}. Thus, the

400 $CaCO_3$ formation rate estimated from the CO_2 gas exchange flux and the decrease in ΔAlk*

401 agree well, in spite of many simplifying assumptions.

402   If this apparent net calcification rate was taking place in coral reefs uniformly spread over

403 the seafloor, the areal rates of CO_2 flux and calcification would be would be ~1.25 mmol m^{-2} d^{-1}

404 (0.46 mol C m^{-2} y^{-1}) and ~0.78 mmol m^{-2} d^{-1} (0.28 mol C m^{-2} y^{-1}), respectively. Studies of air-sea

405 CO_2 fluxes in seawater over healthy coral reef systems have given slightly larger, but

406 comparable results. There are lots of reasons why these comparisons are not valid, but they

407 provide a frame of reference for what fluxes might be possible if corals are producing the

408   $CaCO_3$. For example, the net annual area-specific flux of CO_2 to the atmosphere in Kaneohe

409   Bay, Hawaii was 1.45 mol C m^{-2} y^{-1} (Fagan and Mackenzie, 2007) and 1.24 ± 0.33 mol m^{-2} y^{-1}

410   using a much more extensive data set over a nine-year period (Terlouw et al., 2019). Lonborg et

411   al (2019) calculated an average air-sea flux of CO_2 to the atmosphere in the Great Barrier Reef of

412   1.44 ± 0.15 mmol C m^{-2} d^{-1}. Though pCO_2 in seawater over growing corals varies on diurnal and

413   seasonal time scales, on average it is greater than atmospheric pCO_2 and the fluxes given above

414   are representative.

415   Calculation of the air-sea flux of CO_2 appears to suggest a reasonable rate of calcification

416   but doesn't resolve the question about whether that calcification is occurring in the water column

417   or sediments.

418

419   **4.5 Corals in the Qatari EEZ**

420
421   The magnitude of the apparent rate of net calcification at the sediment water interface

422   calculated from the air-sea flux of CO_2 for the Qatari EEZ is plausible. We know that despite the

423   extreme environmental conditions, the Gulf contains 40 species of *scleractinian* (hard) corals

424   and 35 species of *alcyonacean* (soft) corals (Vaughan et al., 2019). Spatial patterns of corals

425   broadly follow environmental conditions, with the highest diversity occurring near the Strait of

426   Hormuz and along the Iranian coast where environmental conditions are more favorable. Most of

427   the other healthy corals occur along the Trucial Coast of the United Arab Emirates (UAE) in the

428   SW Arabian Gulf. These UAE coral reefs were once extensive but have declined dramatically in

429   the past three decades due to bleaching events (Grizzle et al., 2016).

430   The coral reefs around Qatar were a valuable economic resource in the past. Historically,

431   coral communities around Qatar were among the most widespread in the region. These coral

432   communities were dominated by *Acropora* (staghorn) table corals to water depths of 4-5m and

433   massive *Porites* corals from 5m to 10m. They were described as "extensive" and "lush" (Rezal et

434   al., 2004; Burt et al., 2015).

435   Unfortunately, there has been a general decline in the ecological health of corals in the

436   Qatari region of the Gulf in recent decades. It is hypothesized that net calcification, growth rate

437   and mortality of coral reefs have been adversely affected by bleaching events caused by extreme

438   ocean warming. Severe damage occurred to corals as a result of recurrent bleaching events in

439   1996, 1998, 2002 and 2017 when sea surface temperature (SST) sometimes reached >37°C.

440   These bleaching events resulted in near total loss of all coral from shallow (<3 m) habitats

441   around Qatar. The damage due to bleaching was exacerbated by anthropogenic activities -

442   sedimentation from dredging and pollution from the growing industrial sectors. The near-shore

443   coral communities across much of eastern Qatar have become functionally extinct. Off-shore

444   coral assemblages were also impacted by the bleaching events, but a few isolated, healthy sites

445   exist, like Umm Al-Arshan (Burt et al., 2015) and Halul Island (Abdel-Moati, 2006). However,

446   most off-shore sites (e.g., Fuwaurit and Al-Ashat) are covered by bare rock, sand, algal turfs and

447   dead coral rubble (Burt et al., 2015; Sheppard et al., 2010).

448   The available data on the distribution and health of Qatari corals suggest that formation

449   of $CaCO_3$ in coral reefs is an unlikely origin for the excess pCO_2 in the surface seawater.

450   **4.6 Particulate Ca in the water column**

451   A recent study of the composition of particulate matter in the Qatari EEZ showed that

452   average Ca concentrations in the suspended particulate matter were high (3.6% by mass of

453   particulate matter), and acid soluble (Yigiterhan et al, 2020). Though there is a significant

454   amount of particulate Ca in the water column, its minerology has not been determined.

455 Biological studies reveal that carbonate forming plankton are absent (Quigg et al., 2013;

456 Polikarpov et al., 2016). We considered that the particulate Ca comes from the abundant

457 carbonate-rich atmospheric dust in this region (Yigiterhan et al., 2018). However, using Al as a

458 tracer for dust, and the average Ca/Al ratio in Qatari dust, can only explain about 3% of the

459 particulate Ca in water column particulate matter. So, there is excess $CaCO_3$ in the water column

460 that does not appear to come from either plankton or Qatari dust.

461

462 **4.7 Heterogeneous calcite precipitation (HCP)**

463 It is possible that the excess CO_2 is due to abiological $CaCO_3$ formation in the water

464 column. Such abiological $CaCO_3$ formation (also called heterogeneous calcite precipitation,

465 HCP) was hypothesized by Wurgaft et al. (2016) to occur in the water column of the Red Sea.

466 They interpreted water column data for NTA and NDIC in the Red Sea and the Gulf of Aqaba as

467 indicating that heterogeneous $CaCO_3$ precipitation (HCP) was occurring. As HCP does not

468 normally occur in supersaturated seawater due to inhibition by Mg^{2+} ions (Bischoff, 1977), even

469 with $\Omega > 5$ (Berner, 1975), they argued that this HCP was induced by suspended sediments from

470 flash floods or input of atmospheric dust. Comparisons of the Arabian Gulf and the Red Sea is

471 difficult as the Red Sea is much deeper (>2000m). Nevertheless, the Arabian Gulf and Red Sea

472 are similar in that both have reverse estuarine circulation driven by an increase in salinity due to

473 evaporation in the northern end, growth of corals in shallow waters (Saderne et al., 2019) and

474 large inputs of atmospheric dust. The apparent formation of $CaCO_3$ in the deep waters of the Red

475 Sea (below the euphotic zone) was a key aspect of the argument for abiogenic HCP forming in

476 that region.

477   The case has also been made that abiological, nonskeletal $CaCO_3$ formation occurs in the

478   Grand Bahama Bank, east of the Florida Straits (Swart et al., 2014). In that region, the input of

479   dust from North Africa was hypothesized to play an important role as both heterogeneous

480   nucleation sites and as a source of iron, that would stimulate nitrogen fixation and biological

481   production in this otherwise oligotrophic ocean region.

482

483   5. **Conclusions**

484   pCO_2 is supersaturated relative to atmospheric pCO_2 in the surface seawater of the

485   Arabian Gulf. The relationship between NAlk and NDIC and values of ΔAlk* indicate that

486   substantial $CaCO_3$ precipitation is occurring. The rate of $CaCO_3$ formation calculated from the

487   air-sea flux of CO_2 and the decrease in the tracer ΔAlk* agree well. Removal by coral reefs looks

488   unlikely, as healthy, growing corals are rare due to several recent bleaching events. There is

489   excess, acid soluble, particulate calcium in the water column that cannot be explained as

490   originating from carbonate forming plankton or $CaCO_3$-rich Qatari dust. The saturation states of

491   waters with respect to calcite ($\Omega_{calcite}$ = 4.97 to 6.95) and aragonite ($\Omega_{aragonite}$ = 3.32 to 4.62) are

492   high in the Gulf and perhaps the $CaCO_3$ rich dust can overcome the kinetic inhibition seen in the

493   open ocean. $CaCO_3$ formation in the open ocean is typically biologically mediated. The evidence

494   from this study suggests that heterogeneous calcite precipitation (HCP) could possibly be

495   occurring in the Gulf, as hypothesized previously for the Red Sea. This HCP process may be

496   aided by nucleating sites provided by dust input. If so, inorganic precipitation may play a more

497   important role in coastal regions with significant dust input than previously thought.

498

499   **References**

500

501   Abdel-Moati, M. (2006). Coral Reef Conservation in Qatar, Marine Conservation Forum. EWS-

502   WWF, Abu Dhabi, UAE, pp. 1–34.

503

504   Al-Ansari, E. M. A. S., Rowe, G., Abdel-Moati, M. A. R., Yigiterhan, O., Al-Maslamani, I., Al-

505   Yafei, M. A., Al-Shaikh, I., Upstill-Goddard, R. (2015). Hypoxia in the central Arabian

506   Gulf exclusive economic zone (EEZ) of Qatar during summer season, Estuar. Coast. Shelf S.,

507   159, 60–68, https://doi.org/10.1016/j.ecss.2015.03.022, 2015.

508

509   Berner, R. (1975). The role of magnesium in the crystal growth of calcite and aragonite

510   from sea water. Geochim. Cosmochim. Acta 39, 489–504.

511

512   Bolden I.W., Sachs, J.P. & Gagnon, A.C. (2019). Temporally-variable productivity quotients on

513   a coral atoll: Implications for estimates of reef metabolism. Marine Chemistry 217, 1-13.

514

515   Brewer, P. G. & Dyrssen, D. (1985), Chemical oceanography of the Persian

516   Gulf. Prog. Oceanogr., 14, 41–55

517

518   Burt, J. (2014). The environmental costs of coastal urbanization in the Arabian Gulf. City:

519   Analysis of Urban Trends, Culture, Theory, Policy, Action 18 pp. 760–770.

520

521   Burt, J. A., Smith, E. G., Warren, C., & Dupont, J. (2016). An assessment of Qatar's coral

522   communities in a regional context. Marine Pollution Bulletin, 105, 473–479.

523

524   Carpenter, J. H. (1965). The Chesapeake Bay Institute technique for the Winkler dissolved

525   oxygen method. Limnol. and Oceanogr. 10, 141-143.

526

527   Carter, B.R., Toggweiler, J.R., Key, R.M., & Sarmiento, J.L. (2014). Processes determining the

528   marine alkalinity and calcium carbonate saturation state distributions. Biogeosciences, 11, 7349-

529   7362.

530

531   Cyronak, T., Andersson, A. J., Langdon, C., Albright, R., Bates, N. R., Caldeira, K., et al.

532   (2018). Taking the metabolic pulse of the world's coral reefs. PLoS ONE, 13(1), 1–17.

533   https://doi.org/10.1371/journal.pone.0190872

534

535   Deutsch, C., Sarmiento, J.L., Sigman, D.M., Gruber, N., & Dunne, J.P. (2007) Spatial coupling

536   of nitrogen inputs and losses in the ocean. Nature 445, 163–167

537

538   Dickson, A.G. (1990). Thermodynamics of the dissociation of boric acid in synthetic seawater

539   from 273.15 to 318.15 K. Deep Sea Res.. 37, 755–766. https://doi.org/10.1016/0198-

540   0149(90)90004-F.

541

542   Dickson, A.G., Sabine, C.L., & Christian, J.R. (2007). Guide to best practices for ocean CO2

543   measurements. PICES Special Publication 3.

544

545   Dickson, A.G. & Millero, F.J. (1987). A comparison of the equilibrium constants for the

546   dissociation of carbonic acid in seawater media. Deep Sea Res., 34, 1733–1743.

547   https://doi.org/10.1016/0198-0149(87)90021-5.

548

549   Doney, S.C., Fabry, V.J., Feely, R.A., & Kleypas, J.A. (2009). Ocean acidification: the other

550   CO_2 problem. Annu. Rev. Mar. Sci. 1, 169–192.

551

552   Emerson, S. & Hedges, J. (2012). Chemical Oceanography and the Marine Carbon Cycle.

553   Cambridge University Press. 453pp

554

555   Fagan, K. E. & Mackenzie, F. T. (2007). Air-sea CO2 exchange in a subtropical

556   estuarine-coral reef system, Kaneohe Bay, Oahu, Hawaii. Mar. Chem. 106, 174–191.

557   doi: 10.1016/j.marchem.2007.01.016

558

559   Frankignoulle, M., Canon, C. & Gattuso, J-P. (1994) Marine calcification as a source of carbon

560   dioxide: Positive feedback of increasing atmospheric CO_2. Limnology and Oceanography. 39,

561   458-462

562

563   Grizzle, R.L., Ward, K.M., AlShihi, R.M.S., & Burt, J.A. (2016). Current status of coral reefs in

564   the United Arab Emirates: Distribution, extent, and community structure with implications for

565   management. Marine Pollution Bulletin. 105, 515-523.

566

567   Kampf J. & Sadrinesab, M. (2006). The circulation of the Persian Gulf: a numerical study. Ocean

568   Science, 2, 27-41

569

570   Kanamori, S. & Ikegami, H. (198. Calcium-alkalinity relationship in the North Pacific, J.

571   Oceanogr., 38, 57–62, 1982.

572

573   Lee, K., Kima, T-W., Byrne R.H. , Millero, F.J. , Feely, R.A., & Liu, Y-M. (2010). The universal

574   ratio of boron to chlorinity for the North Pacific and North Atlantic oceans. Geochimica et

575   Cosmochimica Acta, 74, 1801-1811.

576   Liss P.S. & Slater P.G. (1974). Flux of Gases across the Air-Sea Interface. Nature 247, 181-184.

577

578   Lonborg C., Calleja, M.L.I., Fabricius, K,E., Smith, J.N., & Achterberg, E.P. (2019). The Great

579   Barrier Reef: A source of CO_2 to the atmosphere. Marine Chemistry 210, 24-33.

580

581   Mehrbach, C., Culberson, C.H., Hawley, J.E., & Pytkowicx, R.M. (1973). Measurement of the

582   apparent dissociation constants of carbonic acid in seawater at atmospheric pressure.

583   Limnol. Oceanogr. 18, 897–907. https://doi.org/10.4319/lo.1973.18.6.0897.

584

585   Orr, J. C., Fabry, V. J., Aumont, O., Bopp, L., Doney, S. C., Feely, R. A., et al. (2005).

586   Anthropogenic ocean acidification over the twenty-first century and its impact on calcifying

587   organisms, Nature, 437, 681–686

588

589   Orr, J.C., Epitalon, J-M., Dickson, A.G., & Gattuso, J-P. (2018). Routine uncertainty propagation

590   for the marine carbon dioxide system. Marine Chemistry, 207, 84-107

591

592   Parsons T.R., Maita Y., & Lalli, G.M. (1984). A manual of chemical and biological methods for

593   seawater analysis. Pergamon Press, Oxford

594

595   Polikarpov,I., Saburova, M., & Al-Yamani, F. (2016). Diversity and distribution of winter

596   phytoplankton in the Arabian Gulf and the Sea of Oman. Continental Shelf Research, 119, 85-99.

597

598   Quigg, A.,Al-Ansi,M., NourAlDin,N., Wei,C.-L., Nunnally,C.C., Al-Ansari,I.S., Rowe, G.T. et

599   al. (2013). Phytoplankton along the coastal shelf of an oligotrophic hypersaline environment in a

600   semi-enclosed marginal sea: Qatar (Arabian Gulf). Cont. Shelf Res. 60, 1–16.

601

602   Rezai, H., Wilson, S., Claereboudt, M., & Riegl, B., (2004). Coral reef status in the ROPME sea

603   area: Arabian/Persian Gulf, Gulf of Oman and Arabian Sea. In:Wilkinson, C. (Ed.), Status

604   of Coral Reefs of the World: 2004. Australian Institute of Marine Science, Townsville,

605   pp. 155–169.

606

607   Saderne, V., Baldry, K., Anton, A., Agustí, S., & Duarte, C. M. (2019). Characterization of the

608   CO2 system in a coral reef, a seagrass meadow, and a mangrove forest in the central Red Sea.

609   Journal of Geophysical Research: Oceans, 124, 7513–7528.

610   https://doi.org/10.1029/2019JC015266

611

612   Sheppard, C., Al-Husiani, M., Al-Jamali, F., Al-Yamani, F., Baldwin, R., Bishop, J., et al.

613   (2010). The Gulf: a young sea in decline. Mar. Pollut. Bull. 60, 13–38.

614

615   Stumm, W. & Morgan, J.J. (1995) Aquatic Chemistry: Chemical Equilibria and Rates in Natural

616   Waters   3rd Edition. Wiley-Interscience pp, 1040

617

618   Swart, P.K., Oehlen, A.M., Mackenzie, G.J., Eberli, G.P., & Reijmer, J.J.G. (2014) The fertilization

619   of the Bahamas by Saharan Dust: A trigger for carbonate precipitation. Geology, 42: 671-674.

620

621   Terlouw G.J., Knor L.A.C.M., De Carlo E.H., Drupp P.S., Mackenzie F.T., Li Y.H., Sutton A.J.,

622   Plueddemann A.J., & Sabine C.L. (2019). Hawaii Coastal Seawater CO2 Network: A Statistical

623   Evaluation of a Decade of Observations on Tropical Coral Reefs. Front. Mar. Sci. 6, 226.

624   doi: 10.3389/fmars.2019.00226

625

626   Vaughan, G.O., Al-Mansoori, N. & Burt, J.A. (2019). The Arabian Gulf. World Seas: An

627   Environmental Evaluation. Pp, 1-23. https://doi.org/10.1016/B978-0-08-100853-9.00001-4

628   Elsevier.

629

630   Wanninkhof, R. (1992). Relationship between wind speed and gas exchange over the ocean. J.

631   Geophys. Res. 97, 7373–7382.

632   Ware, J. R., Smith S.V. & Reaka-Kudla, M.L. (1991) Coral reefs: sources or sinks of

633   atmospheric CO_2? Coral Reefs, 11, 127-130

634

635   Wolf-Gladrow, D.A., Zeebe, R.E., Klaas, C., Koertzinger, A., & Dickson, A.G., (2007). Total

636   alkalinity: the explicit conservative expression and its application to biogeochemical processes.

637   Mar. Chem. 106, 287–300.

638

639   Wurgaft E., Steiner, Z., Luz, B., & Lazar, B. (2016). Evidence for inorganic precipitation of $CaCO_3$

640   on suspended solids in the open water of the Red Sea. Marine Chemistry, 186, 145-155.

641

642   \Yao H., McCutcheon M.R., Staaryk C.J., & Hu X. (2020). Hydrologic controls on CO_2

643   chemistry and flux in subtropical lagoonal estuaries of the northwestern Gulf of Mexico. Limnol

644   Oceanogr. 65: 1380-1398

645

646   Yigiterhan O., Alfoldy B.Z, Giamberini M., Turner J.C., Al-Ansari E.S., Abdel-Moati M.A., Al-

647   Maslamani I.A., Kotb M.M., Elobaid E.A., Hassan H.A., Obbard J.P., & Murray J.W., (2018).

648   Geochemical Composition of Aeolian Dust and Surface Deposits from the Qatar Peninsula.

649   Chemical Geology 476, 24-45

650

651   Yigiterhan O. Al-Ansari, E.M.A.S., Nelson, A., Abdel-Moati, M.A.R., Turner, J., Alsaadi, H.A.,

652   Paul, B., Al-Maslamani, I.A., Al-Yafei, M.A.A.A., & Murray, J.W. (2020). Trace element

653   composition of size-fractionated suspended particulate matter samples from the Qatari Exclusive

654   Economic Zone of the Arabian Gulf: the role of atmospheric dust. Biogeosciences. 17, 381-401.

655

656

Competing Interests

None of the authors have financial and personal competing interests to declare.

Author Contributions

J.W.M. and O.Y. designed the research. Samples were collected by J.A-T, O.Y., E.A-A, and C.S.
Hydrographic data was processed by C.S. Nutrient analyses were conducted by J.A-T. J.W.M.
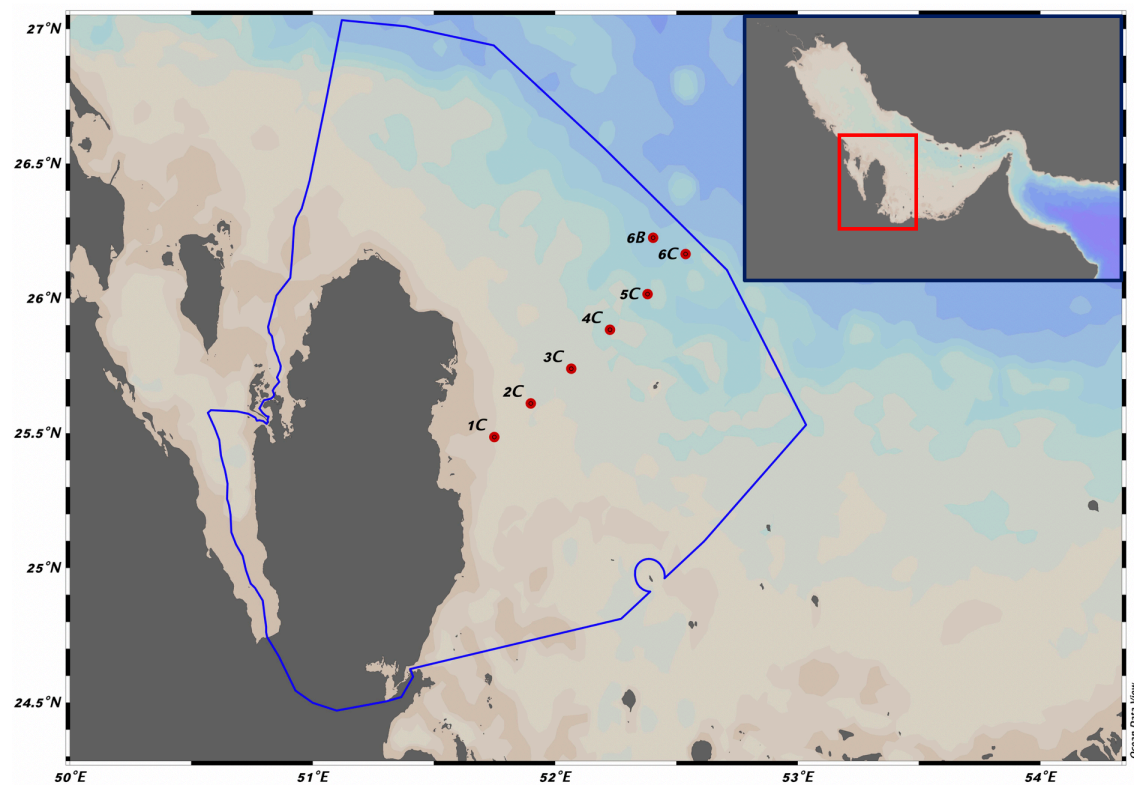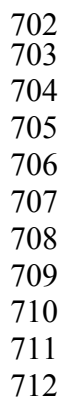wrote the manuscript. All authors edited the manuscript.

Table 1. Water column data from November 2018 and May 2019. The units for O_2, NO_3, soluble reactive phosphate (SRP), SiO_2, DIC and TA are all $\mu mol\ kg^{-1}$ The units for pCO_2 are μatm. The grand averages for the combined data sets are DIC = $2180 \pm 40 \mu mol\ kg^{-1}$. Alk = $2532 \pm 30\ \mu mol\ kg^{-1}$ and $pCO_2 = 459 \pm 61\ \mu atm$. Samples from the surface, middle and bottom of the water column are colored blue, orange and green, respectively

Data from November 2018

Station	Depth	Temperature	Salinity	O2	NO3	PO4	SiO2	DIC	ALK	pCO2	pHcalc
1C	1.8	24.621	40.983	197	1.18	0.08	1.07	2065	2426	390	8.047
1C	10.3	24.458	40.994	196	1.61	0.33	1.38	2085	2415	438	8.004
2C	1.5	25.550	40.766	198	1.39	0.20	0.50	2128	2517	387	8.064
2C	22.3	24.900	40.855	191	1.09	0.06	0.64	2134	2514	391	8.059
3C	1.4	26.683	40.641	201	0.75	0.07	0.40	2197	2531	514	7.967
3C	15	26.314	40.625	195	1.27	0.37	0.50	2208	2528	537	7.951
3C	30	25.756	40.667	176	0.77	0.19	1.00	2150	2528	410	8.046
4C	1.8	26.819	40.565	202	0.57	0.16	1.44	2150	2530	426	8.033
4C	12.4	26.686	40.557	198	1.25	0.19	1.19	2154	2533	426	8.033
4C	36.9	26.669	40.557	190	1.28	0.20	1.85	2152			
5C	1.7	26.845	40.604	193	1.29	0.17	1.34	2213	2533	549	7.944
5C	15	26.822	40.602	191	1.77	0.31	0.90	2214	2530	561	7.936
5C	30.2	26.791	40.594	185	1.52	0.22	1.33	2148			
5C	51	26.796	40.595	184	1.68	0.22	0.98	2149	2535	416	8.041
6C	1.6	26.770	40.479	187	1.54	0.36	1.38	2230	2536	583	7.925
6C	18.3	26.773	40.478	188	1.89	0.26	0.84	2161	2540	431	8.031
6C	33.5	26.821	40.520	183	1.18	0.29	0.67	2224	2538	569	7.933
6C	53.3	26.843	40.531	181	2.40	0.23	1.40	2223	2538	564	7.936
6B	1.4	26.212	40.295	191	1.48	0.24	0.68	2164	2601	351	8.112
6B	20.4	26.219	40.291	187	1.66	0.21	0.72	2167	2542	429	8.037
6B	40	26.217	40.292	184	1.63	0.21	0.79	2233	2539	572	7.935
6B	57.5	26.218	40.290	182	2.03	0.28	3.65	2164	2543	422	8.042
6B	1.4	26.212	40.295	191	1.49	0.93	1.65	2232	2538	573	7.933
6B	57.5	26.218	40.290	182	1.86	0.22	2.56	2235	2540	575	7.933
Average								2174	2526	478	7.997
Std. Dev								47	38	80	0.058

Data from May 2019

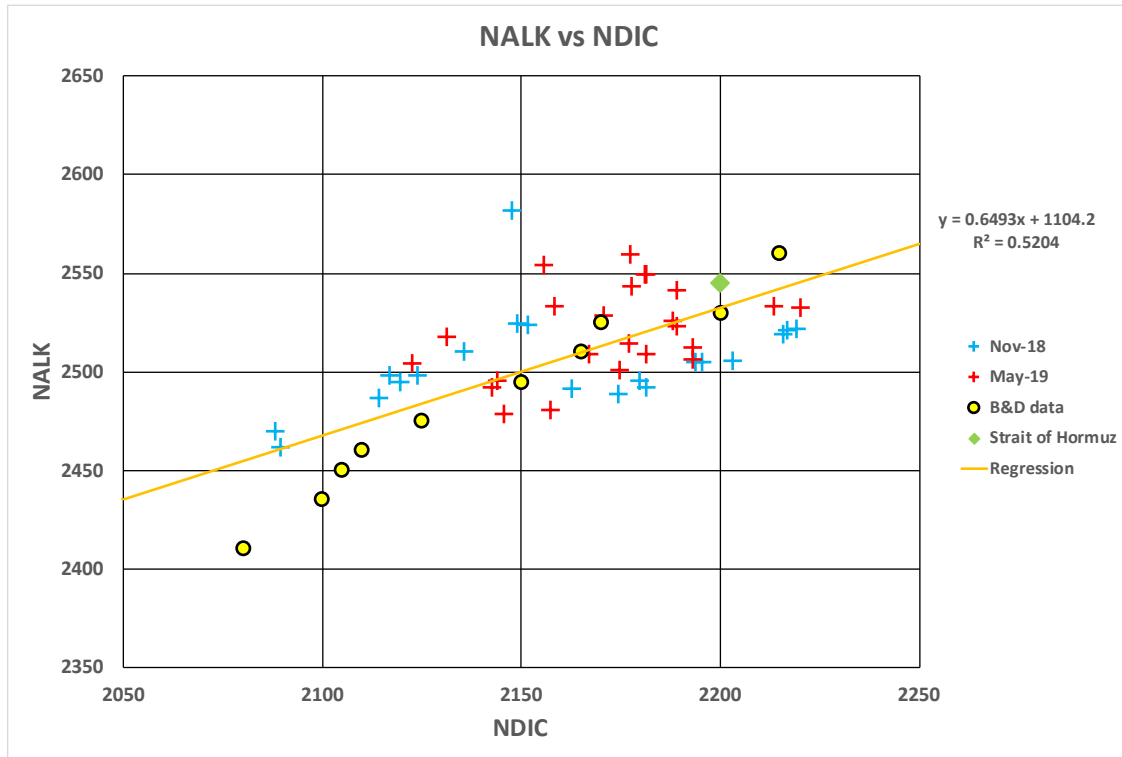| Station	Depth	Temperature	Salinity	O2	NO3	PO4	SiO2	DIC	ALK	pCO2	pHcalc
1C	1.7	27.043	41.026	190	0.54	0.35	2.64	2198	2556	483	7.988
1C	10	26.730	40.999	186	0.62	0.73	1.17	2197	2557	474	7.995
2C	1.6	27.599	40.757	207	4.22	1.44	2.21	2163	2552	434	8.027
2C	21.8	25.138	41.128	177	0.63	0.05	0.73	2206	2548	478	7.991
3C	1.7	27.527	40.451	211	0.86	0.05	0.63	2155	2546	424	8.038
3C	15.3	24.380	40.862	202	2.12	0.46	1.04	2214	2563	453	8.016
3C	29.6	24.505	41.201	166	0.94	0.36	1.05	2222	2555	485	7.987
4C	1.8	27.320	39.597	199	2.35	0.52	0.98	2134	2528	406	8.06
4C	15.8	23.387	40.310	229	1.65	0.29	1.24	2188	2548	409	8.056
4C	37	23.797	40.747	177	1.70	0.54	1.64	2215	2547	470	8.002
5C	1.6	27.124	39.274	161	1.76	2.29	1.60	2138	2513	429	8.042
5C	15.8	23.601	39.870	169	1.27	0.47	1.30	2171	2535	400	8.067
5C	32.6	22.600	40.190	138	1.61	0.57	2.63	2200	2535	434	8.035
5C	50.6	22.185	40.275	128	1.44	0.71	3.08	2203	2543	422	8.046
6C	1.8	27.263	39.304	131	2.25	0.14	0.77	2143	2505	450	8.024
6C	14.4	25.015	39.640	146	0.96	0.55	0.93	2169	2518	443	8.03
6C	33.3	21.252	40.075	143	3.54	0.80	2.81	2218	2538	441	8.032
6C	58.5	21.421	40.593	115	3.24	0.74	4.20	2214	2546	427	8.04
6B	1.7	27.297	39.361	185	1.51	0.22	0.63	2146	2509	452	8.023
6B	18.2	23.136	39.889	181	1.30	0.32	0.68	2152	2526	373	8.09
6B	34.4	21.400	40.032	137	2.17	1.13	1.90	2222	2535	456	8.021
6B	58.5	20.794	40.624	119	4.14	0.85	4.05	2227	2545	442	8.027
6B	1.7	27.297	39.361					2142	2474	500	7.983
6B	58.5	20.794	40.624					2227	2551	432	8.036
Average								2186	2536	442	8.027
Std. Dev								32	21	30	0.027

30

687
688
689
690
Figure 1: Station locations sampled in November 2018 and May 2019 in the Qatari Exclusive Economic Zone (EEZ) of Qatar in the Arabian Gulf

693
694

698   **Figure 2. Alk versus DIC in the Exclusive Economic Zone (EEZ) of Qatar in the Arabian**
699   **Gulf. The units for Alk and DIC are µmol kg^{-1}. The data point for 1977 from the Strait of**
700   **Hormuz is from Brewer and Dyrssen (1985)**
701

702
703
704
705
706
707
708
709
710
711
712

713 **Figure 3. NAlk versus NDIC in the Qatari EEZ of the Arabian Gulf in November**
714 **2018 and May 2019. Data from 1977 for the entire Arabian Gulf and Strait of**
715 **Hormuz by Brewer and Dyrssen (1985) are shown for comparison. The units for**
716 **NAlk and NDIC are μmol kg^{-1}. The slope of the best fit regression (0.65)**
717 **corresponds to a ΔCaCO$_3$ / ΔOrgC removal ratio of ~1:2.**
718

719
720
721
722
723
724
725
726
727
728
729
730
731

732 **Figure 4. ΔAlk* in the Qatari EEZ, calculated as the difference between the value**
733 **of Alk* at individual stations and the value for the Strait of Hormuz. ΔAlk* is**
734 **plotted versus distance from the Strait of Hormuz. The gradual decrease in ΔAlk***
735 **indicates progressive precipitation of CaCO₃.**
736
737

738
739
740
741
742
743
744
745
746
747